Accepted Manuscript

Spectra of high energy electron precipitation and atmospheric ionization rates retrieval from balloon measurements

Irina Mironova, Galina Bazilevskaya, Gennady Kovaltsov, Anton Artamonov, Eugene Rozanov, Alexander Mishev, Vladimir Makhmutov, Arseniy Karagodin, Ksenia Golubenko

PII: S0048-9697(19)33161-4
DOI: https://doi.org/10.1016/j.scitotenv.2019.07.048
Reference: STOTEN 33242

To appear in: *Science of the Total Environment*

Received date: 30 April 2019
Revised date: 1 July 2019
Accepted date: 3 July 2019

Please cite this article as: I. Mironova, G. Bazilevskaya, G. Kovaltsov, et al., Spectra of high energy electron precipitation and atmospheric ionization rates retrieval from balloon measurements, Science of the Total Environment, https://doi.org/10.1016/j.scitotenv.2019.07.048

Spectra of high energy electron precipitation and atmospheric ionization rates retrieval from balloon measurements

Irina Mironova[a,*], Galina Bazilevskaya[b], Gennady Kovaltsov[c], Anton Artamonov[d], Eugene Rozanov[e,f], Alexander Mishev[g,h], Vladimir Makhmutov[b], Arseniy Karagodin[a], Ksenia Golubenko[a]

[a]*St. Petersburg State University, St. Petersburg, Russia*
[b]*Lebedev Physical Institute, Russian Academy of Science, Moscow, Russia*
[c]*Ioffe Physical -Technical Institute, St. Petersburg, Russia*
[d]*Research Institute for Space Medicine Federal Research Clinical Center of Federal Biomedical Agency of Russia, Moscow, Russia*
[e]*PMOD/WRC and IAC ETHZ, Davos Dorf, Switzerland*
[f]*Western Department of Pushkov Institute of Terrestrial Magnetism, Ionosphere and Radio Waves Propagation, Russian Academy of Sciences, Kaliningrad, Russia*
[g]*Space Climate Research Unit, University of Oulu, Finland*
[h]*Sodankylä Geophysical Observatory, Oulu, Finland*

Abstract

The bremsstrahlung from high and relativistic energy electron precipitation (HEEP) measured with balloon based instruments provides information on energy spectra and fluence of the precipitating energetic electrons allowing calculations of the atmospheric ionization. HEEP from the outer radiation belt at the subauroral region causes an increase in the ionization rates down to about 20 km altitudes. We study the variability in the ionization rate using the balloon observations of secondary bremsstrahlung initiated by HEEP. For the first time the changes of atmospheric ionization rates on an hourly and minute time scale at different altitudes was retrieved from balloon observations. These new

[☆]Spectra calculation and ionization retrieval from balloon measurements of high energy electron precipitation

[*]Corresponding author

Email addresses: i.a.mironova@spbu.ru (Irina Mironova), bazilevskayaga@lebedev.ru (Galina Bazilevskaya), gen.koval@mail.ru (Gennady Kovaltsov), anton.art.an@gmail.com (Anton Artamonov), eugene.rozanov@pmodwrc.ch (Eugene Rozanov), alexander.mishev@oulu.fi (Alexander Mishev), makhmutv@lebedev.ru (Vladimir Makhmutov), karars94@mail.ru (Arseniy Karagodin), golubksen@yandex.ru (Ksenia Golubenko)

highlights are important for atmospheric electricity that is sensitive to the local condition in the atmosphere including the local ionization rate.

Keywords: high and relativistic energy electron precipitation (HEEP), polar atmosphere, balloon observations, electron spectra and ionization rates

1. Introduction

There are various types of high energy precipitating particles inducing atmospheric ionization and transformation of the structure, composition, and dynamics of the polar atmosphere. The ionization of the polar atmosphere is mostly caused by protons of solar and galactic origins as well as auroral electrons and electrons precipitating from the radiation belts. Their energies vary from eV to GeV. Depending on the type and energy, these particles can penetrate and impact different atmospheric layers (e.g. Mironova et al., 2015, and references therein).

In the polar regions, the induced ionization initiates chemical changes affecting ozone and temperature distributions (e.g. Rozanov et al., 2012; Sinnhuber et al., 2016). Reviews of Füllekrug et al. (2013); Kumar et al. (2018) showed the importance of ionization for electrical discharge processes, electromagnetic emissions etc. Energetic particle precipitation can also contribute to the vertical component of the fair weather electric field at the ground level at high latitudes (Füllekrug et al., 2013) and increase the electrical conductivity as well as decrease both the vertical and horizontal electric field components (Kokorowski et al., 2006). The papers (Mironova et al., 2008, 2012; Mironova and Usoskin, 2013, 2014) showed variability of aerosol optical and microphysical parameters under strong increase of ionization rates in the polar winter stratosphere. A paper by Schlegel and Füllekrug (1999) presents a systematic study of Schumann resonance parameters during high-energy particle precipitation events. It is demonstrated that growth of ionization leads to an increase in the resonance frequency and to a decrease in the damping of the first Schumann resonance, as derived from measurements at Antarctica. Several papers showed a strong increase of atmospheric conductivity at balloon altitudes due to the ionization induced by solar energetic particle precipitation (e.g. Rycroft et al., 2008; Kokorowski et al., 2012). All these results clearly demonstrate importance of precipitating particles in the polar atmosphere, specifically for local parameters of global electrical circuit. The new Atmosphere-Space Interactions Monitor (ASIM) mission (Østgaard et al., 2019) on the International Space Station is specially organized for investigation of global effects of relativistic electron precipitation during geomagnetic storms and lightning induced precipitation.

All information presented above shows importance of knowledge of atmospheric ionization induced by energetic particle precipitation. In the present paper we focus on polar regions of the middle atmosphere where forcing from high and relativistic energy electrons precipitating from the outer radiation belt is more important in comparison to other sources of precipitating particles (Mironova et al., 2015).

The energy spectra and ionization due to precipitating electrons can be assessed using balloon observations, which allow to perform measurements of secondary radiation emitted by the precipitating electrons. The balloon observations cover energy range of precipitating electrons up to several MeV and allow studing the high energy and relativistic electron precipitation (HEEP). The energy range of HEEP covers the diapason of so-called middle energy electrons (MEE) from 30 keV to 1 MeV (Matthes et al., 2017, e.g.) as well as the energy of relativistic electrons that starts from about 500 keV up to tens MeV. Balloon based devices register bremsstrahlung from HEEP providing information on energy spectra of precipitating energetic electrons (Makhmutov et al., 2006; Millan et al., 2013; Woodger et al., 2015; Makhmutov et al., 2016) and further on the atmospheric ionization.

Here, we will concentrate on the analysis of selected HEEP events as observed by balloons in the polar region. We discuss variability of the precipitating electron energy spectra and corresponding variability of ionization rates at different altitudes on the minute and hourly time scales.

2. HEEP balloon observations

Since 1957, the Lebedev Physical Institute has been carrying out regular balloon measurements of the fluxes of ionizing particles at different latitudes and altitudes in the atmosphere (Charakhch'yan, 1964; Stozhkov et al., 2009), which, among other things, make it possible to detect precipitations of magnetospheric electrons with energy above 100 keV from the outer radiation belt. Electrons that precipitate into the polar atmosphere are absorbed at altitudes above 50 km. However, HEEP generate bremsstrahlung X-rays which penetrate the polar atmosphere down to altitudes of the order of 20 km (Makhmutov et al., 2006; Makhmutov et al., 2016; Artamonov et al., 2016, 2017) and can be recorded by a balloon based device. The observed data are collected at the site of the Lebedev Physical Institute ($http://sites.lebedev.ru/ru/DNS\_FIAN/479.html$).

The balloon measurements are carried out with a standard radiosound shown in Figures 1. The charged particle detector consists of two Geiger counters with 0.05 g/cm^2 steel walls arranged as a vertical telescope, with a 7 mm (2 g/cm^2) thick filter inserted between the counters. The operating sizes of the counters are 9.8 cm length and 1.8 cm in diameter. The geometrical factor of a single counter depends on particle angular distribution. For the isotropic flux, it is 16 cm^2. Geiger counter counts the number of ionizing particles that fell into it, i.e., protons with energy E $\geq$5 MeV, electrons with E $\geq$ 200 keV, muons with E $\geq$ 1 MeV, and X-rays with E $\geq$ 20 keV. A telescope records a vertical flux of charged particles within a solid angle of about 1 sr: electrons with energy E $\geq$ 5 MeV, protons with E $\geq$ 30 MeV, and muons with E $\geq$15 MeV. Both the omnidirectional and vertical fluxes of charged particles in the atmosphere are measured. A radio pulse caused by a charged particle passing through a counter or a telescope is transmitted to the ground-level receiver. In addition, the residual air pressure (the atmospheric depth) is measured. The 700 g radiosound is lifted by a meteorological balloon with the peak altitude of around 30-35 km. The electronics design of the radiosound has been refined in the course of the long-term experiment yet the type and configuration of detectors have

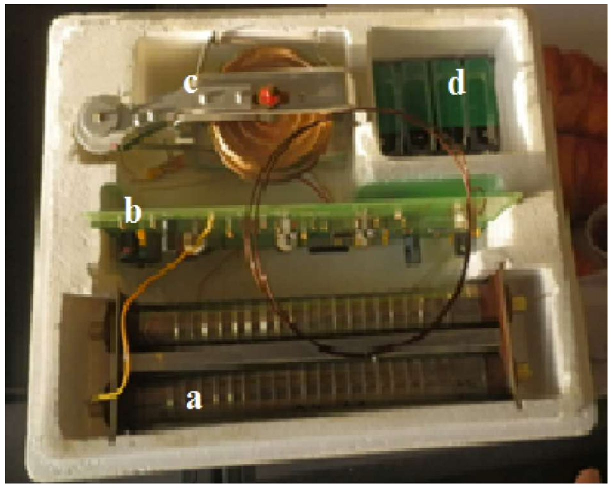

Figure 1: A standard radiosound for energetic charged particles observation in the atmosphere, consisting of Geiger counters (a), electronic plate with high-frequency transmitter (b), altitude sensor (c), power supply (d).

remained unchanged during the whole period of the measurements. The main problem of long-term monitoring is the maintenance of measurements at a constant efficiency level by a careful detector calibration, for details see Bazilevskaya and Svirzhevskaya (1998). Reliability and homogeneity of the charged particle data series is proved by excellent consistency of the primary galactic cosmic ray spectrum in the energy interval of 10^8 eV - 10^9 eV as obtained in the balloon experiment with cosmic ray fluxes in the adjacent energy intervals derived from the spacecraft and the ground-based measurements during the whole period of observations from 1957 up to now (Stozhkov et al., 2009).

The galactic cosmic rays generate the secondary radiation which has a maximum effect at altitudes around 20–25 km. Intrusion into the atmosphere of solar or magnetospheric particles leads to an increase in the balloon count rates with altitude. Until 2012, a radiosoundes carried a counter telescope that was sensitive to the solar protons but not sensitive to the bremsstrahlung from HEEP.

That made it possible to separate the precipitation of solar energetic particles and HEEP into the atmosphere since both phenomena lead to an increase in the count rate in the stratosphere (Bazilevskaya et al., 2010). Currently, we use GOES satellite data ($https://satdat.ngdc.noaa.gov/sem/goes/data/new\_avg$) to eliminate solar energetic particle precipitation. Effect of galactic cosmic rays is removed by subtracting a background from the previous flight without energetic particle precipitation. The energy of precipitating electrons can be estimated from the depth of penetration of the bremsstrahlung X-ray radiation into the atmosphere. Approximately 55% of the HEEP events detected in the atmosphere are caused by electrons with $E >$ about 200 - 1300 keV. HEEP with $E < 200$ keV was observed in 9% of events, and HEEP with $E > 1300$ keV in 36% of events.

In this paper, we investigate variability of spectra and altitudinal profiles of ionization rates using the data that were obtained during the balloon measurements in the Murmansk region from 1957 till present days. From 1957 to mid of 2001, balloon were launched at Olenya, $68^0 57^{'}$N 33^0 $03^{'}$E. McIlwain parameter L of the site changed during this time from 5.5 to 5.7. Till the beginning of 1990ies the measurements were performed every day and even up to 10 times per week in 1968-1982. Around 60% of the observations at the altitude above 25 km were made during about 10-11 MLT, and 40%, during 13-17 MLT. In 2001, the observations moved to Apatity, $67^0 33^{'}$N 33^0 $20^{'}$E, the McIlwain parameter L = 5.2 – 5.3, the launching rate is 3 times per week, observation time is about 15 MLT. More than 550 HEEP events have been registered from 1961 to the present time.

3. Variability of the HEEP spectra in the polar atmosphere

The long-term in situ observations in the Murmansk region (Makhmutov et al., 2016) allow studing he HEEP occurrence rate variability on different time scales. There are several basic patterns of variability in the HEEP occurrence rate, such as the 11-year cycle, 27-day, and seasonal variations (Bazilevskaya et al., 2017a,b, 2018). Strong maxima in the occurrence rate of the HEEP events were observed in 1967, 1974, 1984, 1994, 2003, and 2015, during the decline phases of the 11-year solar activity cycle showing a close relationship with the periods of the high-speed solar wind streams. Similar origin has a 27-day recurrent variation. The seasonal variation with maxima close to the equinoxes is typical for several geomagnetic phenomena (e.g. McPherron et al., 2013). Strong connection of the HEEP occurrence rate were found with interplanetary (magnetic field strength and its B_z component, solar wind velocity, plasma density, pressure, temperature, etc.) and geomagnetic (AE, K_p, Dst) parameters (Bazilevskaya et al., 2017b). The HEEP events tend to occur in clusters during geomagnetic storms with long-lasting recovery phase (Bazilevskaya et al., 2017b, 2018). A series begins with arrival of a highspeed solar wind stream and an abrupt decrease of the Dst index. In the case of negative B_z component of interplanetary magnetic field, an enhanced amount of disturbed plasma enters the magnetosphere changing the geomagnetic field configuration. Geomagnetic storms are accompanied by interplanetary wave penetration into the magnetosphere and generation of new magnetospheric waves. Enhancement of wave-particle interactions leads to strong particle dynamic in the outer radiation belt (e.g. Eastwood et al., 2015). Electron acceleration and loss are the competing processes resulting in fast filling and depletion of particle population. A series of the HEEP events continues during the recovery phase of a geomagnetic storm. Connection between HEEP and any of interplanetary and geomagnetic parameters is ambiguous because of numerous and diverse interrelation of processes involved in the radiation belt dynamics. That is why using only one or two parameters as triggering the HEEP occurrence, such as A_p and Dst indexes (van de Kamp et al., 2016) can be only a first approximation. Not all HEEP events are governed by geomagnetic storms, some are due to substorm activity (Bazilevskaya et al., 2018). On the other hand, strong radiation belt dynamic may not be accompanied by HEEP, because majority electrons can escape from the magnetosphere to the interplanetary space (Bazilevskaya et al., 2017b; Xiang et al., 2017). In general, features of the HEEP as observed in the stratosphere are consistent with the radiation belt dynamics as explored by recent instruments, for instance, SAMPEX (Blum et al., 2015), Van Allen Probe (Murphy et al., 2018).

Here we address variability in the precipitating electron flux values that are their intrinsic feature (e.g. Clilverd et al., 2010). The time scale of the observed variability is several minutes because we accumulate data during one minute interval or several hours due to an opportunity to record a HEEP during two sequential balloon flights at the same day. Actually, in approximately 50% of events, the count rates increase with altitude rather smoothly, and this enables us to robustly extract the electron energy spectrum from the X-ray absorption in the atmosphere. However, there are many HEEP events with very fluctuating count rate, sometimes of oscillating type. In this case, we can only find an average spectrum and the limits of the flux values. In case of long-lasting flights, when the variability of precipitating particle fluxes cannot be ignored, we evaluate the spectrum separately for each part with smooth changes in count rate.

The characteristic of primary precipitating electrons is evaluated using the GEANT 4 simulations (Makhmutov et al., 2016). The differential spectra of the electron fluxes are fitted by an exponential law:

$$F_e(E) = A_e * exp(-E/E_0), \tag{1}$$

where E_0 is characteristic energy of spectra. Range of E_0 is about 10 keV – 1000 keV. A_e - parameter of the flux of incident electrons in keV^{-1} cm^{-2} s^{-1}.

Figures 2 - 4 illustrate changes in the precipitating particle fluxes as observed during a balloon flight. Panel a) of Figures 2 - 4 display the count rate vs atmospheric pressure during the balloon flight when HEEP was recorded. Subtracting the background due to galactic cosmic rays as observed during the preceding balloon flight without precipitation we obtain $\geq$ 20 keV photon flux (arbitrary units) at different heights, that is shown in panel b). The scattering of results reflects the HEEP variability. In order to estimate the accuracy of primary electron spectrum derived from balloon observations, we put the upper and lower limits on the measured records, trying to consider the majority of observation data. The upper and lower lines in the panel b) of Figures 2 - 4 demonstrate the maximum uncertainties in the particle flux estimation. These limits are used for the calculations of the maximum and minimum electron energy spectra using the method described in (Makhmutov et al., 2016), see panel c) in Figures 2 - 4. Panel d) in Figures 2 - 4 presents the altitude profiles of ionization induced by the HEEP as calculated in the Section 4.

The flight on 22 September 2003, Figure 2, is an example of "a quiet" precipitation while the assumption of small variability in the electron spectrum seems to be reasonable. Although the flux fluctuations are small, they exceed the statistical errors. As can be seen in Fig. 2, panels c) and d), the changes in the energy spectrum of precipitating electrons and in the ionization rate were negligible.

During the long-lasting flight on 19 September 2003, Figure 3, the balloon stayed at the altitude higher than 25 km for about 1 hour. At 09:16 UT, an abrupt change in the dependence of the Geiger tube count rate on the atmospheric depth occurred, but afterward, at 09:23 UT, the character of this dependence resumed. In this case, the electron spectrum was evaluated separately for different parts of observations Figures 3, panel c). Variability was small within each selected interval, but it was noticeable between the intervals.

In the case of the strong fluctuations in the electron fluxes, such as on 30 July 2003, Figure 4, we can only evaluate an average spectrum. In this case we assume that the energy spectrum of electrons did not change during the flight, and only the particle flux fluctuated as it is seen in panel b) of Figure 4. Putting the limits on the fluctuations results in a noticeable variation in the HEEP induced ionization rates, which we show as colored corridors in panels c) and d) of Figure 4.

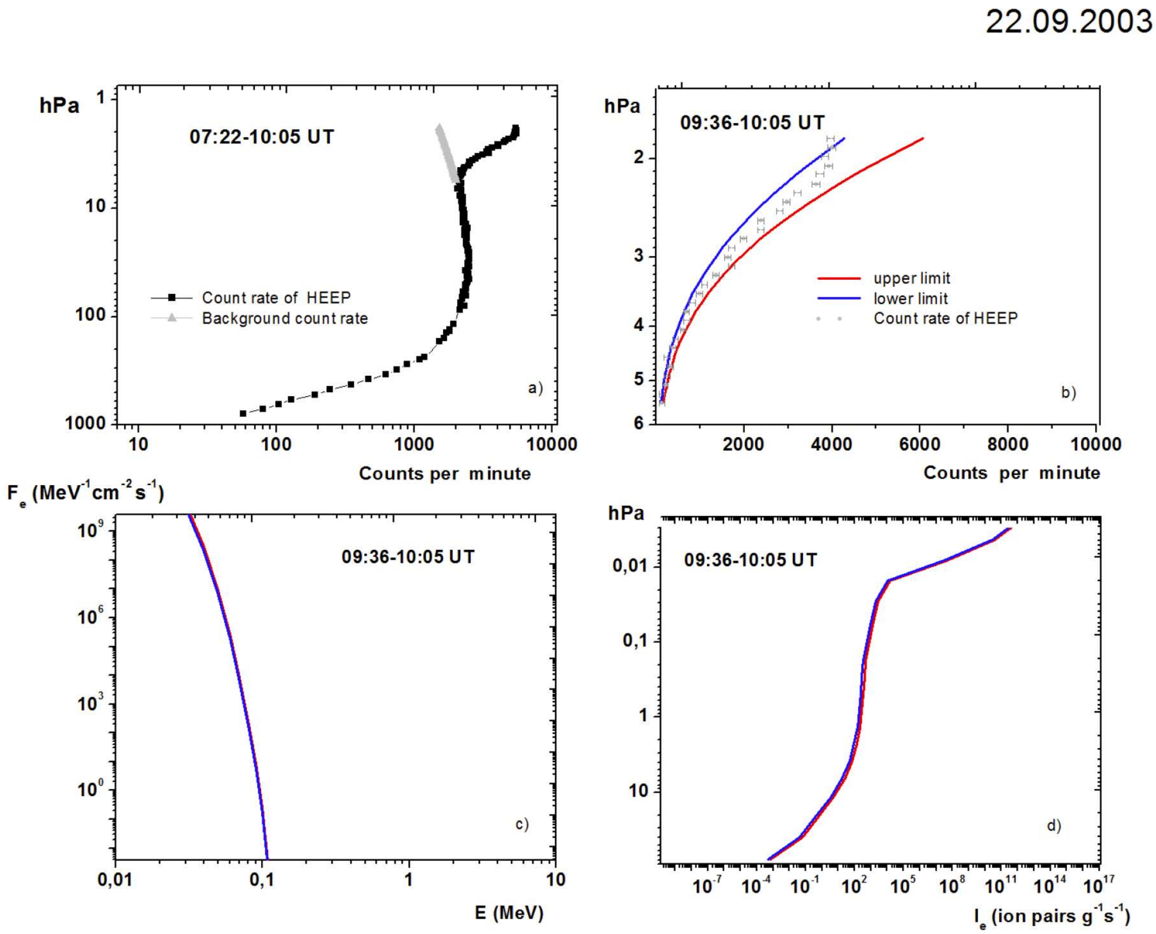

Figure 2: High and relativistic energy electron precipitation observed during the balloon flight on 22 September 2003. a) Black squares are the count rate of the Geiger tube during the whole balloon flight on 22 September 2003. Grey line is a background from galactic cosmic rays as measured in the previous balloon flight. b) Count rate due to X-ray fluxes; the errors are statistical. Blue and red lines indicate upper and lower limits of fluxes considering the majority of data. c) Electron energy spectra F_e corresponding to the maximum and minimum limits of the X-ray fluxes. d) Ionization rates I_e retrieved from the spectra on panel c). Variability in the spectrum and ionization rates were negligible.

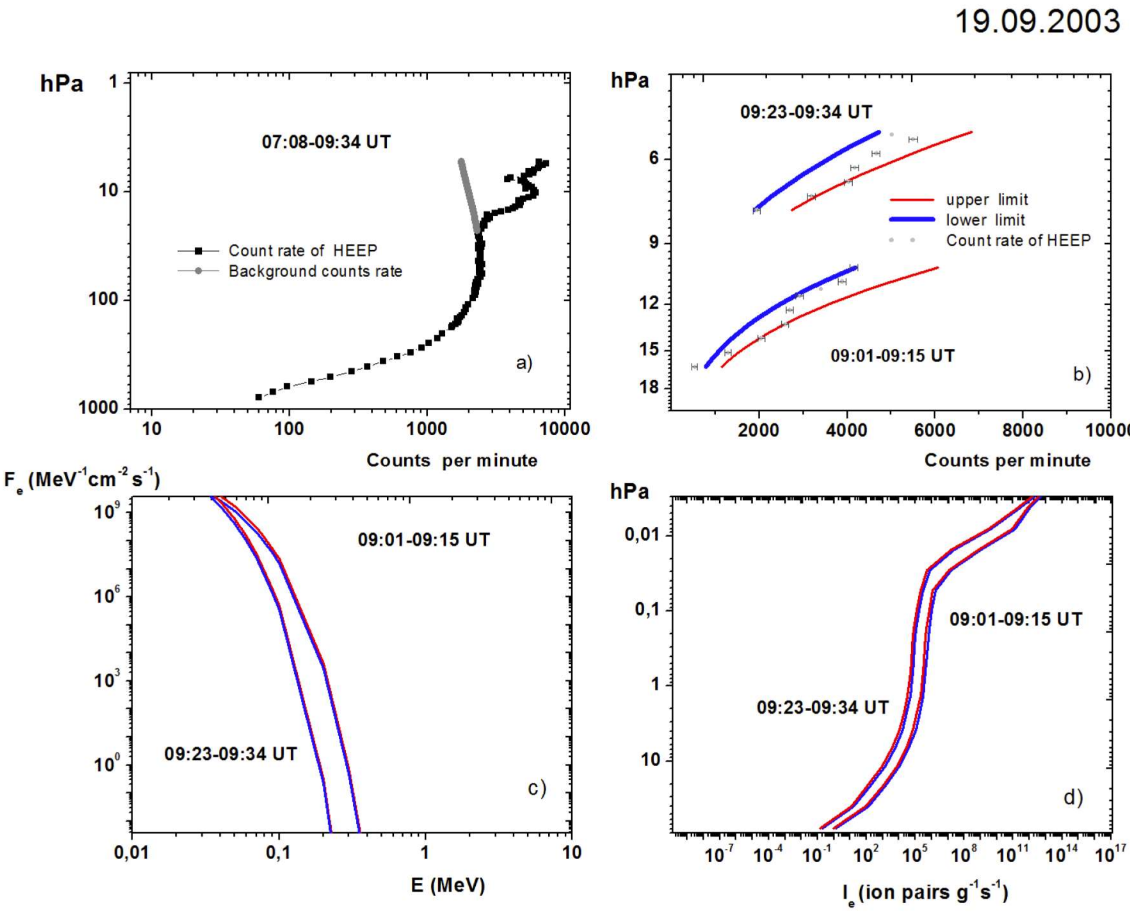

Figure 3: The same as in Figure 2 but for the long-lasting balloon flight on 19 September 2003. The time intervals 09:01- 09:15 UT and 09:23 - 09:34 UT were treated separately.

4. Ionization rates during HEEP at different altitudes

Distribution of the ionization rates in the atmosphere depends on the flux and energy spectra of the precipitating particles. Calculation of ionization rates requires knowledge of the energy spectra and ionization yield functions. For the computation of ionization rates we used a recently proposed model based on ionization yield function formalism and corresponding information about HEEP spectra (Artamonov et al., 2016, 2017). The ionization yield function

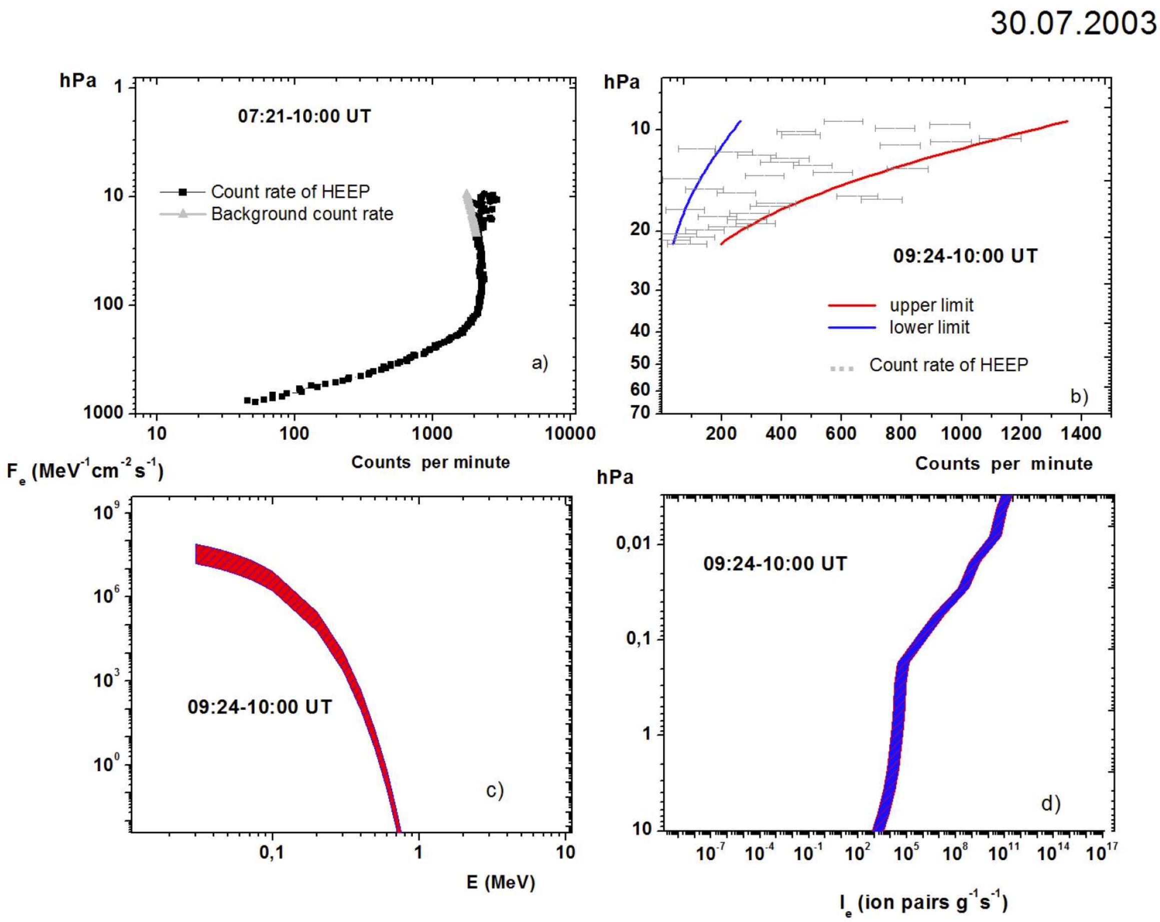

Figure 4: The same as in Figure 2 but for the balloon flight on 30 July 2003. Strong fluctuations in count rate during the flight led to substantial variability in the derived differential spectra of the electron fluxes F_e and ionization rates I_e induced that are shown by the colored corridors.

$Y_e(x, E)$ (ion pairs cm^2 g $^{-1}$) at the atmospheric depth x (g cm^{-2}), is a number of ion pairs created by one precipitating electron with the initial energy E at the upper boundary of atmosphere. In this study we used modified ionization yield functions for mono-energetic electrons with initial energy from 30 keV to 10 MeV. The direct ionization by primary electrons as well as the secondary bremsstrahlung electromagnetic emissions are both considered in the model.

The ionization rates (ion pairs per g $^{-1}$ s $^{-1}$) can be computed as:

$$I_e(x) = \int J_e(x,E)dE, \tag{2}$$

where $J_e(x,E)$ is a production function:

$$J_e(x,E) = Y_e(x,E) * F_e(E), \tag{3}$$

and $F_e(E)$ is a spectrum of precipitating electrons at the top of atmosphere. In our calculations we consider exponential spectra of HEEP, see Eq. 1

Figure 5 shows yield functions $Y_e(x,E)$ for precipitating electrons with initial energy E. One can see a flattening at high altitudes. This feature is due to dominating direct ionization by primary electrons. The sharp decrease at lower altitudes is related to the transition from direct ionization to ionization via bremsstrahlung.

Figure 6 a), upper panel, illustrates energy dependence of yield functions, $Y_e(x,E)$, at different atmospheric pressure levels and demonstrates transitions from direct ionization at high energies to bremsstrahlung ionization at lower energies. The bremsstrahlung ionization dominates at pressure levels deeper than several hPa. In fact, X- ray fluxes at polar latitudes are measured during HEEP in a pressure interval from several hPa to a few tens of hPa.

In Fig. 6 (panels b), production functions $J_e(x,E)$ are shown at different pressure levels for $E_0 = 300$ keV. The production function represents the differential ionization function defined as a product of the ionization yield function and a given spectrum of precipitating electrons. The ordinate axis on the panel b) has a logarithmic scale, and on the panel c) it has a linear scale. All curves are normalized to their corresponding maximum. Red line on panel (b) depicts HEEP energy spectra in arbitrary units. In the region of higher energies, the production function reflects the energy dependence on the spectrum of precipitating electrons, which can be seen when comparing the curves for production functions with the red curve on the panel b) of Figure 6. The combination of a sharp increase in the production function at the transition from bremsstrahlung ionization to direct ionization from the incident primary electrons leads to the

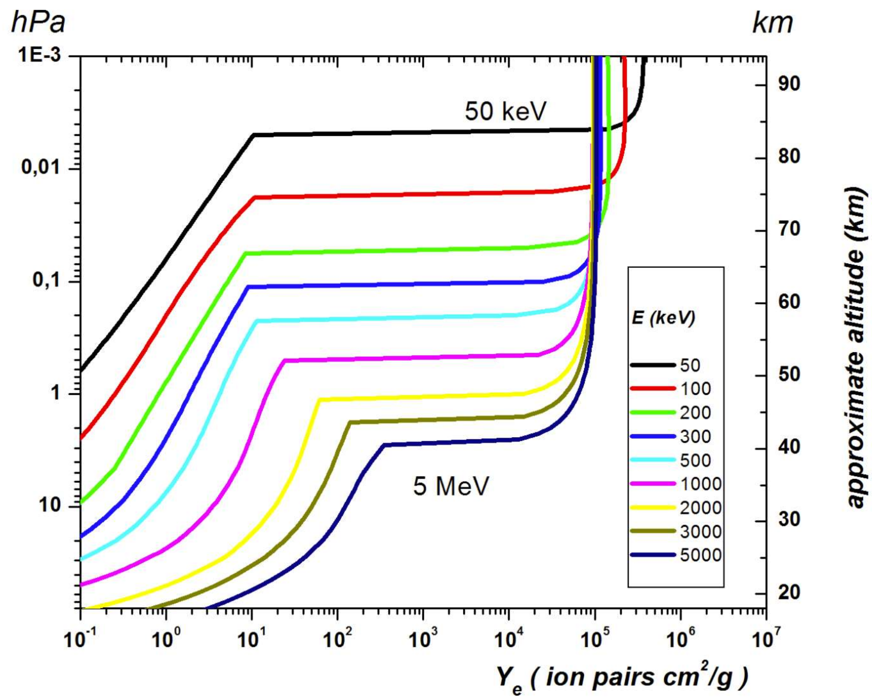

Figure 5: Yield functions $Y_e(x, E)$ of mono-energetic precipitating electrons for unit isotropic flux at the top of the atmosphere. Lines with different symbols correspond to $Y_e(x, E)$ calculated for different initial electron energies. Atmospheric pressure 1 hPa is about 1 g/cm^2 of atmospheric depth x.

appearance of clear maxima of the production function, see Fig. 6 the panels b) – c). The position of these maxima determines the regions of the effective energy of the primary electrons for ionization at a given height. For example, at pressure level 0.01 hPa (for electron spectrum with E_0= 300 keV) the effective energy range of primary electrons correspond about 700 keV, see Fig. 6 panel c). In Fig. 7 ionization rates are calculated for selected characteristic energies of HEEP spectra, see Eq. 1: E_0 = 30 keV; 100 keV; 300 keV and 1000 keV. The whole range of HEEP spectra covers energies from several keV up to 10 MeV that defined as limits of integration, see Eq. 2. All curves are normalized to corresponding values $I_e(x)$ at 10^{-2} hPa. The ionization rates can be divided

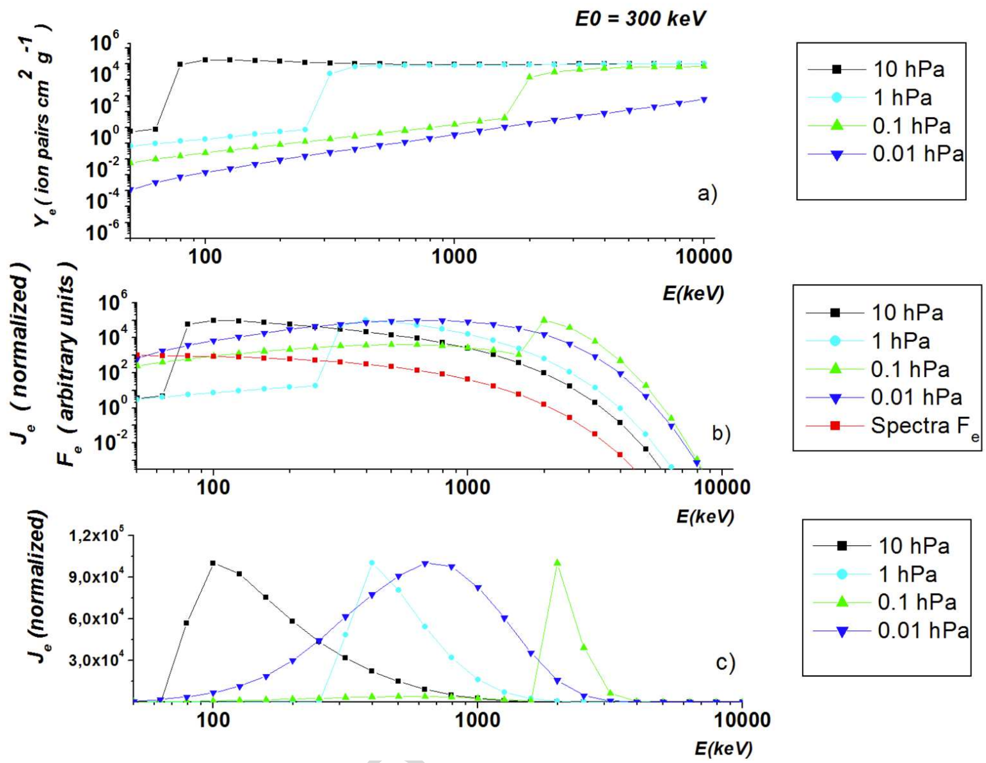

Figure 6: Upper panel (a) shows energy dependence of yield functions at different pressure levels. Panels below (b) demonstrate the normalized production functions $J_e(x, E)$ for characteristic energy of electron spectum E_0 at different pressure levels. The ordinate axis on the panel (b) has a logarithmic scale, and on the panel (c) it has a linear scale. Red lines represent precipitating electron spectra $F_e(E)$.

into two classes connected with direct ionization by primary electrons or ionization by secondary bremsstrahlung radiation. This reflects main properties of yield functions. Variability of altitudinal profiles of ionization rates for different characteristic energies E_0 is determined by variability of production function $J_e(x, E)$ via spectrum of precipitating electrons.

In the Section 3 we showed spectra of HEEP during 19 and 22 September 2003, as well as during 30 July 2003. Panel d), Figures 2 - 4 presents altitudinal profiles of ionization rates for these HEEPs. For the long-lasting flight on 19 September 2003 the uncertainty in $I_e(x)$ for each part of the flight was negligible,

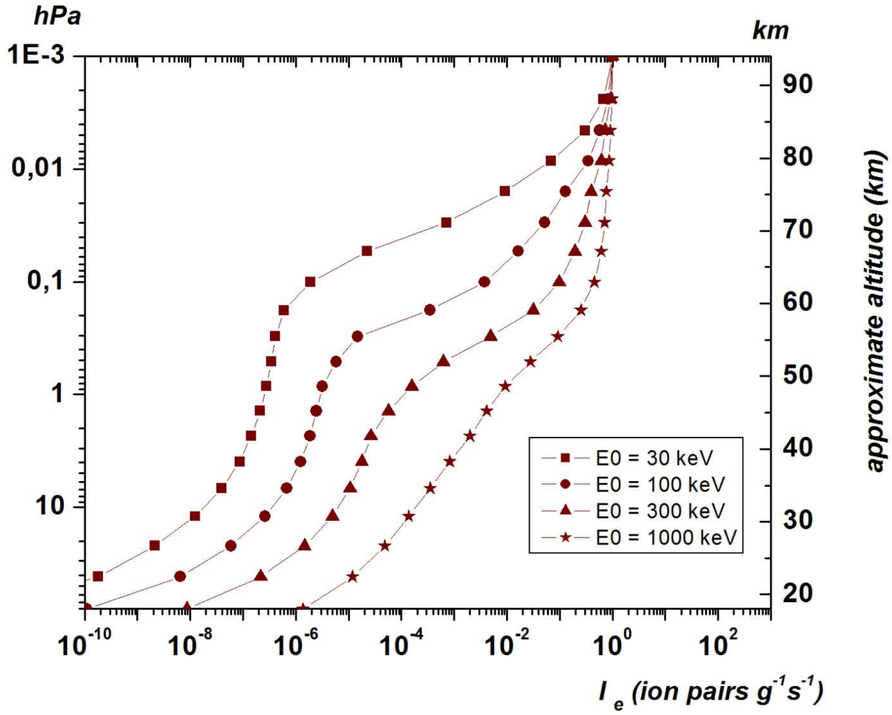

Figure 7: Normalized ionization rates $I_e(x)$ calculated for selected characteristic energy of HEEP spectra E_0 = 30 keV; 100 keV; 300 keV and 1000 keV.

but ionization rate was significantly higher during the earlier part of the flight, see Figure 3, panel d). This suggests that ionization rates during HEEP can vary over tens minutes.

From mid 1960ies until mid 1980ies balloon launches were often performed twice a day, in the morning and afternoon. It should be noted that our observations do not provide information about the real start and end of the HEEP event, as we can record precipitation only while the balloon is aloft. However, we can state, that in the most of observations, the HEEP did not last more than 6 hours, as it was as a rule recorded only in the morning or in the afternoon flight. However, in several events, the HEEP was recorded during both flights, although we cannot distinguish if HEEP related to the same or to the different episodes. In any case, these results enable us to see the HEEP variability on the several hours time scale. Figure 8 gives examples of the electron energy spectra and induced ionization rates calculated for two flights on the same day. One can see that various situations are possible. Changes in the electron spectra and ionization rates $I_e(x)$ on 25 May 1982 were small, while they were substantial on other days. The morning spectrum on 29 September 1972 was softer than the afternoon spectrum, but the opposite case was observed on 21 April 1973. As a rule, variability on the hourly scale is clearly higher than on the minute scale. Certainly, the data are scarce and can be only considered as examples.

5. Conclusion

The atmospheric electricity features may be sensitive to the local condition in the atmosphere including the local ionization rate. For this reason, the HEEP variability in the given location is important. Such information cannot be taken from the satellite observations because the spacecraft moves too fast over each region and covers larger area with lower resolution. The balloon measurements are relevant for this task since balloons are being launched regularly at the same locations. The characteristics of HEEP obtained from measurements of secondary bremsstrahlung in balloon experiments show high day to day variability (Makhmutov et al., 2016; Mironova et al., 2019). Here, for the first time, we present calculations of variability in atmospheric ionization rates on the time scales of minutes and hours. Substantial changes in precipitating electron fluxes can occur both during one balloon flight and during two balloon flights performed on the same day. On the other hand, in the case of two daily balloon launches, as a rule, HEEP was observed only in one of them, that proves the existence of strong changes in ionization rate on the time scale of 6 hours and longer. Whereas the present knowledge about temporal and spatial variations of HEEP is not complete enough the balloon observations shed some light on the variability of ionization rates induced by HEEP.

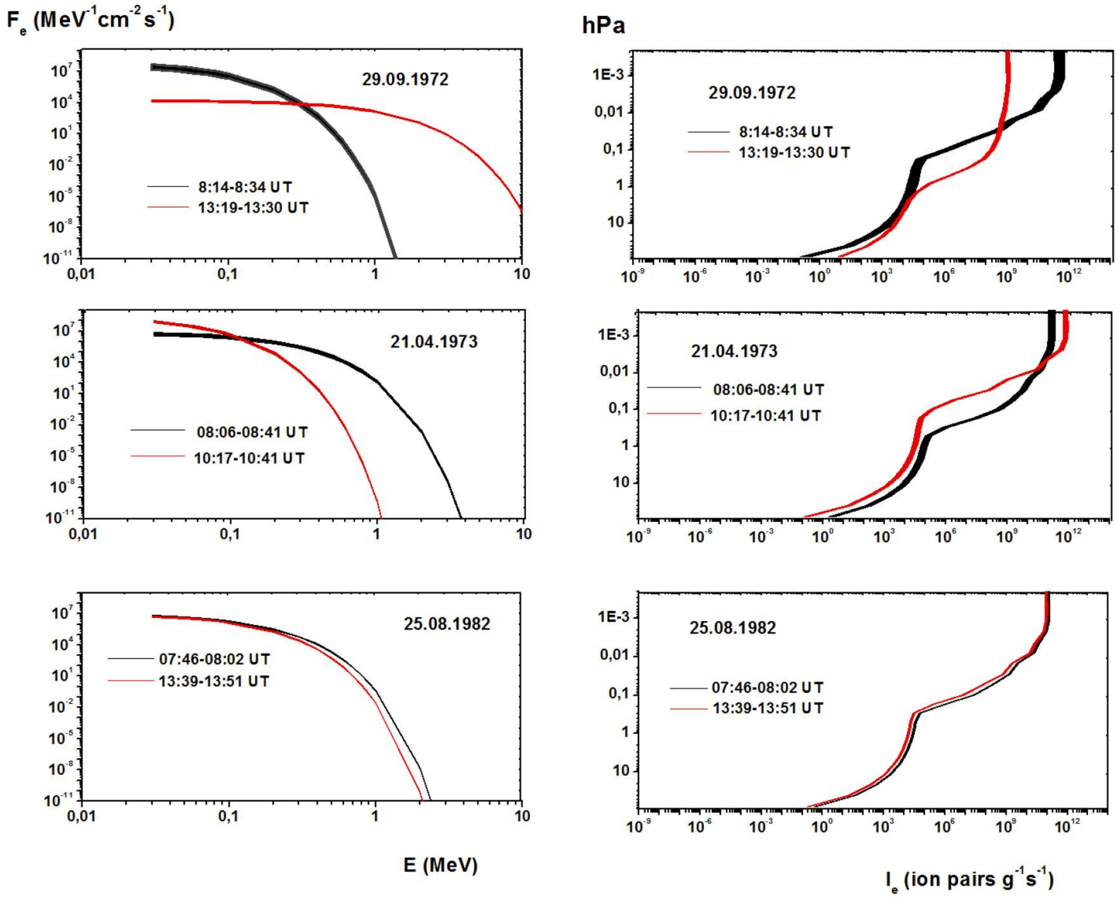

Figure 8: Examples of precipitating electron energy spectra (left panels) and of atmospheric ionization rates (right panels) caused by HEEP events observed in two balloon flights performed on the same day. The morning data are black lines, and the afternoon data, red lines. Time of observations is indicated.

Acknowledgements

310 IM acknowledges for support of St. Petersburg State University through the Grant COLLAB2019_1, id: 37715474 and id: 37715267. ER participated in the data analysis and his work was supported by the Russian Science Foundation (grant no. 17-17-01060). Balloon measurements were supported by the Russian

Academy of Sciences and the Russian Foundation for Basic Research (e.g., grant no. 16-02-00100). AM was supported by the Academy of Finland (project no. 272157, Center of Excellence ReSoLVE). AA, GK, IM, AM thank for support the Academy of Finland (project HEAIM no. 314982 and no. 316223). This work was done in the frame of the COST Action CA15211 "Atmospheric Electricity Network: coupling with the Earth System, climate and biological systems" and the ISSI and the ISSI-BJ project "Relativistic electron precipitation and its atmospheric effect".

References

Artamonov, A., Mironova, I., Kovaltsov, G., Mishev, A., Plotnikov, E., Konstantinova, N., 2017. Calculation of atmospheric ionization induced by relativistic electrons with non - vertical precipitation: update of model CRAC:EPII. Adv. Space Res. 59, 2295 – 2300. doi:https://doi.org/10.1016/j.asr.2017.02.019.

Artamonov, A.A., Mishev, A.L., Usoskin, I.G., 2016. Model CRAC:EPII for atmospheric ionization due to precipitating electrons: Yield function and applications. J. Geophys. Res. 121, 1736–1743. doi:10.1002/2015JA022276.

Bazilevskaya, G.A., Kalinin, M.S., Krainev, M.B., Makhmutov, V.S., Svirzhevskaya, A.K., Svirzhevsky, N.S., Stozhkov, Y.I., Gvozdevsky, B.B., 2018. Characteristics of the Energetic Electron Precipitation and Magnetospheric Conditions in 1994. Geomag. and Aeronomy 58, 483–492. doi:10.1134/S0016793218040023.

Bazilevskaya, G.A., Kalinin, M.S., Krainev, M.B., Makhmutov, V.S., Svirzhevskaya, A.K., Svirzhevsky, N.S., Stozhkov, Y.I., Philippov, M.V., Balabin, Y.V., Gvozdevsky, B.B., 2017a. Precipitation of magnetospheric electrons into the Earth's atmosphere and the electrons of the outer radiation belt. Bulletin of the Russian Academy of Sciences, Physics 81, 215–218. doi:10.3103/S1062873817020071.

Bazilevskaya, G.A., Kalinin, M.S., Kvashnin, A.N., Krainev, M.B., Makhmutov, V.S., Svirzhevskaya, A.K., Svirzhevsky, N.S., Stozhkov, Y.I., Balabin, Y.V., Gvozdevsky, B.B., 2017b. Precipitation of energetic magnetospheric electrons and accompanying solar wind characteristics. Geomag. and Aeronomy 57, 147–155. doi:10.1134/S0016793217020025.

Bazilevskaya, G.A., Makhmutov, V.S., Stozhkov, Y.I., Svirzhevskaya, A.K., Svirzhevsky, N.S., 2010. Solar proton events recorded in the stratosphere during cosmic ray balloon observations in 1957-2008. Adv. Space Res. 45, 603–613. doi:10.1016/j.asr.2009.11.009.

Bazilevskaya, G.A., Svirzhevskaya, A.K., 1998. On The Stratospheric Measurements of Cosmic Rays. Space Sci. Rev. 85, 431–521.

Blum, L., Li, X., Denton, M., 2015. Rapid MeV electron precipitation as observed by SAMPEX/HILT during high-speed stream-driven storms. J. Geophys. Res. 120, 3783–3794. doi:10.1002/2014JA020633.

Charakhch'yan, A.N., 1964. Reviews of Topical Problems: Investigation of Stratosphere Cosmic Ray Intensity Fluctuations Induced by Processes on the Sun. Soviet Physics Uspekhi 7, 358–374. doi:10.1070/PU1964v007n03ABEH003670.

Clilverd, M.A., Rodger, C.J., Moffat-Griffin, T., Spanswick, E., Breen, P., Menk, F.W., Grew, R.S., Hayashi, K., Mann, I.R., 2010. Energetic outer radiation belt electron precipitation during recurrent solar activity. J. Geophys. Res. 115, A08323. doi:10.1029/2009JA015204.

Eastwood, J.P., Hietala, H., Toth, G., Phan, T.D., Fujimoto, M., 2015. What Controls the Structure and Dynamics of Earth's Magnetosphere? Space Sci. Rev. 188, 251–286. doi:10.1007/s11214-014-0050-x.

Füllekrug, M., Diver, D., Pinçon, J.L., Phelps, A.D.R., Bourdon, A., Helling, C., Blanc, E., Honary, F., Harrison, R.G., Sauvaud, J.A., Renard, J.B., Lester, M., Rycroft, M., Kosch, M., Horne, R.B., Soula, S., Gaffet, S., 2013. Energetic

Charged Particles Above Thunderclouds. Surveys in Geophysics 34, 1–41. doi:10.1007/s10712-012-9205-z.

van de Kamp, M., Seppälä, A., Clilverd, M.A., Rodger, C.J., Verronen, P.T., Whittaker, I.C., 2016. A model providing long-term data sets of energetic electron precipitation during geomagnetic storms. J. Geophys. Res. , n/a–n/adoi:10.1002/2015JD024212. 2015JD024212.

Kokorowski, M., Sample, J.G., Holzworth, R.H., Bering, E.A., Bale, S.D., Blake, J.B., Collier, A.B., Hughes, A.R.W., Lay, E., Lin, R.P., McCarthy, M.P., Millan, R.M., Moraal, H., O'Brien, T.P., Parks, G.K., Pulupa, M., Reddell, B.D., Smith, D.M., Stoker, P.H., Woodger, L., 2006. Rapid fluctuations of stratospheric electric field following a solar energetic particle event. Geophys. Res. Lett. 33, L20105. doi:10.1029/2006GL027718.

Kokorowski, M., Seppälä, A., Sample, J.G., Holzworth, R.H., McCarthy, M.P., Bering, E.A., Turunen, E., 2012. Atmosphere-ionosphere conductivity enhancements during a hard solar energetic particle event. J. Geophys. Res. 117, A05319. doi:10.1029/2011JA017363.

Kumar, S., Siingh, D., Singh, R.P., Singh, A.K., Kamra, A.K., 2018. Lightning Discharges, Cosmic Rays and Climate. Surveys in Geophysics 39, 861–899. doi:10.1007/s10712-018-9469-z.

Makhmutov, V., Bazilevskaya, G., Stozhkov, Y., Svirzhevskaya, A., Svirzhevsky, N., 2016. Catalogue of electron precipitation events as observed in the long-duration cosmic ray balloon experiment. J. Atmos. Solar-Terr. Phys. 149, 258 – 276. doi:http://dx.doi.org/10.1016/j.jastp.2015.12.006.

Makhmutov, V.S., Bazilevskaya, G.A., Desorgher, L., Flückiger, E., 2006. Precipitating electron events in October 2003 as observed in the polar atmosphere. Adv. Space Res. 38, 1642–1646. doi:10.1016/j.asr.2006.01.016.

Matthes, K., Funke, B., Andersson, M.E., Barnard, L., Beer, J., Charbonneau, P., Clilverd, M.A., Dudok de Wit, T., Haberreiter, M., Hendry, A., Jackman, C.H., Kretzschmar, M., Kruschke, T., Kunze, M., Langematz, U., Marsh, D.R., Maycock, A.C., Misios, S., Rodger, C.J., Scaife, A.A., Seppälä, A., Shangguan, M., Sinnhuber, M., Tourpali, K., Usoskin, I., van de Kamp, M., Verronen, P.T., Versick, S., 2017. Solar forcing for CMIP6 (v3.2). Geos. Model Dev. 10, 2247–2302. doi:10.5194/gmd-10-2247-2017.

McPherron, R.L., Baker, D.N., Pulkkinen, T.I., Hsu, T.S., Kissinger, J., Chu, X., 2013. Changes in solar wind-magnetosphere coupling with solar cycle, season, and time relative to stream interfaces. J. Atmos. Solar-Terr. Phys. 99, 1–13. doi:10.1016/j.jastp.2012.09.003.

Millan, R.M., McCarthy, M.P., Sample, J.G., Smith, D.M., Thompson, L.D., McGaw, D.G., Woodger, L.A., Hewitt, J.G., Comess, M.D., Yando, K.B., Liang, A.X., Anderson, B.A., Knezek, N.R., Rexroad, W.Z., Scheiman, J.M., Bowers, G.S., Halford, A.J., Collier, A.B., Clilverd, M.A., Lin, R.P., Hudson, M.K., 2013. The Balloon Array for RBSP Relativistic Electron Losses (BARREL). Space Sci. Rev. 179, 503–530. doi:10.1007/s11214-013-9971-z.

Mironova, I.A., Aplin, K.L., Arnold, F., Bazilevskaya, G.A., Harrison, R.G., Krivolutsky, A.A., Nicoll, K.A., Rozanov, E.V., Turunen, E., Usoskin, I.G., 2015. Energetic Particle Influence on the Earth's Atmosphere. Space Sci. Rev. 194, 1–96. doi:10.1007/s11214-015-0185-4.

Mironova, I.A., Artamonov, A.A., Bazilevskaya, G.A., Rozanov, E.V., Kovaltsov, G.A., Makhmutov, V.S., Mishev, A.L., Karagodin, A.V., 2019. Ionization of the Polar Atmosphere by Energetic Electron Precipitation Retrieved From Balloon Measurements. Geophys. Res. Lett. 46, 990–996. doi:10.1029/2018GL079421.

Mironova, I.A., Desorgher, L., Usoskin, I.G., Flückiger, E.O., Bütikofer, R., 2008. Variations of aerosol optical properties during the extreme solar event in January 2005. Geophys. Res. Lett. 35, L18610. doi:10.1029/2008GL035120.

Mironova, I.A., Usoskin, I.G., 2013. Possible effect of extreme solar energetic particle events of September-October 1989 on polar stratospheric aerosols: a case study. Atmos. Chem. Phys. 13, 8543–8550. doi:10.5194/acp-13-8543-2013.

Mironova, I.A., Usoskin, I.G., 2014. Possible effect of strong solar energetic particle events on polar stratospheric aerosol: a summary of observational results. Environmental Research Letters 9, 015002. doi:10.1088/1748-9326/9/1/015002.

Mironova, I.A., Usoskin, I.G., Kovaltsov, G.A., Petelina, S.V., 2012. Possible effect of extreme solar energetic particle event of 20 January 2005 on polar stratospheric aerosols: direct observational evidence. Atmos. Chem. Phys. 12, 769–778. doi:10.5194/acp-12-769-2012.

Murphy, K.R., Watt, C.E.J., Mann, I.R., Jonathan Rae, I., Sibeck, D.G., Boyd, A.J., Forsyth, C.F., Turner, D.L., Claudepierre, S.G., Baker, D.N., Spence, H.E., Reeves, G.D., Blake, J.B., Fennell, J., 2018. The Global Statistical Response of the Outer Radiation Belt During Geomagnetic Storms. Geophys. Res. Lett. 45, 3783–3792. doi:10.1002/2017GL076674.

Østgaard, N., Balling, J.E., Bjørnsen, T., Brauer, P., Budtz-Jørgensen, C., Bujwan, W., Carlson, B., Christiansen, F., Connell, P., Eyles, C., Fehlker, D., Genov, G., Grudziński, P., Kochkin, P., Kohfeldt, A., Kuvvetli, I., Thomsen, P.L., Pedersen, S.M., Navarro-Gonzalez, J., Neubert, T., Njøten, K., Orleanski, P., Qureshi, B.H., Cenkeramaddi, L.R., Reglero, V., Reina, M., Rodrigo, J.M., Rostad, M., Sabau, M.D., Kristensen, S.S., Skogseide, Y., Solberg, A., Stadsnes, J., Ullaland , K., Yang, S., 2019. The Modular X- and Gamma-Ray Sensor (MXGS) of the ASIM Payload on the International Space Station. Space Sci. Rev. 215, 23. doi:10.1007/s11214-018-0573-7.

Rozanov, E., Calisto, M., Egorova, T., Peter, T., Schmutz, W., 2012. Influence of the Precipitating Energetic Particles on Atmospheric Chemistry and Climate. Surv. Geophys. 33, 483–501. doi:10.1007/s10712-012-9192-0.

Rycroft, M.J., Harrison, R.G., Nicoll, K.A., Mareev, E.A., 2008. An Overview of Earth's Global Electric Circuit and Atmospheric Conductivity. Space Sci. Rev. 137, 83–105. doi:10.1007/s11214-008-9368-6.

Schlegel, K., Füllekrug, M., 1999. Schumann resonance parameter changes during high-energy particle precipitation. J. Geophys. Res. 104, 10111–10118. doi:10.1029/1999JA900056.

Sinnhuber, M., Friederich, F., Bender, S., Burrows, J.P., 2016. The response of mesospheric NO to geomagnetic forcing in 2002-2012 as seen by SCIAMACHY. J. Geophys. Res. 121, 3603–3620. doi:10.1002/2015JA022284.

Stozhkov, Y.I., Svirzhevsky, N.S., Bazilevskaya, G.A., Kvashnin, A.N., Makhmutov, V.S., Svirzhevskaya, A.K., 2009. Long-term (50 years) measurements of cosmic ray fluxes in the atmosphere. Adv. Space Res. 44, 1124–1137. doi:10.1016/j.asr.2008.10.038.

Woodger, L.A., Halford, A.J., Millan, R.M., McCarthy, M.P., Smith, D.M., Bowers, G.S., Sample, J.G., Anderson, B.R., Liang, X., 2015. A summary of the BARREL campaigns: Technique for studying electron precipitation. J. Geophys. Res. 120, 4922–4935. doi:10.1002/2014JA020874.

Xiang, Z., Tu, W., Li, X., Ni, B., Morley, S.K., Baker, D.N., 2017. Understanding the Mechanisms of Radiation Belt Dropouts Observed by Van Allen Probes. J. Geophys. Res. 122, 9858–9879. doi:10.1002/2017JA024487.

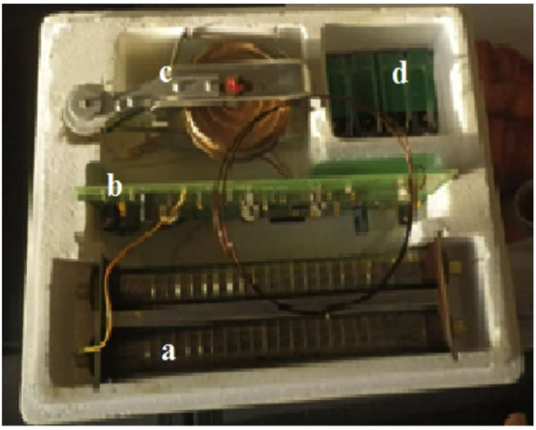

Figure 1

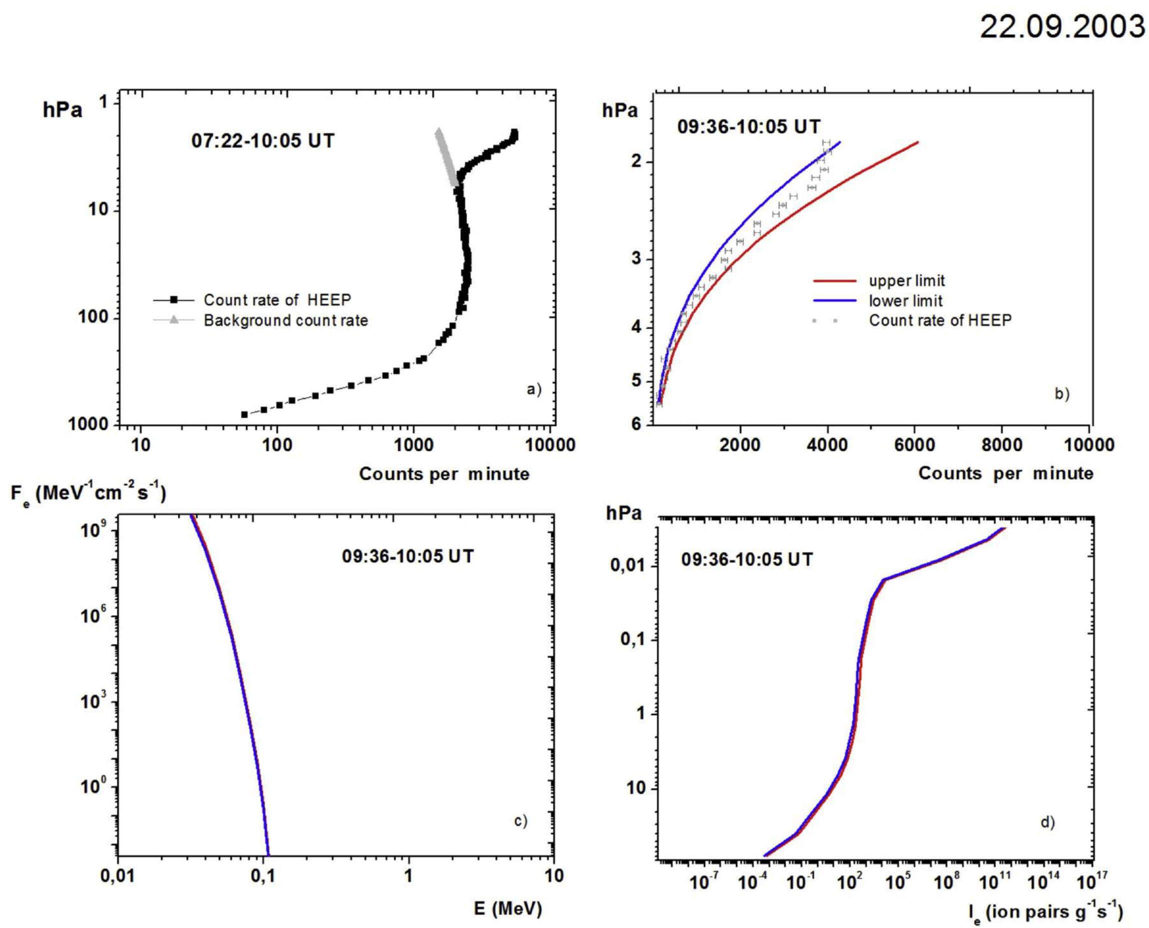
22.09.2003
hPa
07:22-10:05 UT
Count rate of HEEP
Background count rate
a)
Counts per minute
09:36-10:05 UT
upper limit
lower limit
Count rate of HEEP
b)
Counts per minute
F_e (MeV^-1 cm^-2 s^-1)
09:36-10:05 UT
c)
E (MeV)
hPa
09:36-10:05 UT
d)
I_e (ion pairs g^-1 s^-1)

Figure 2

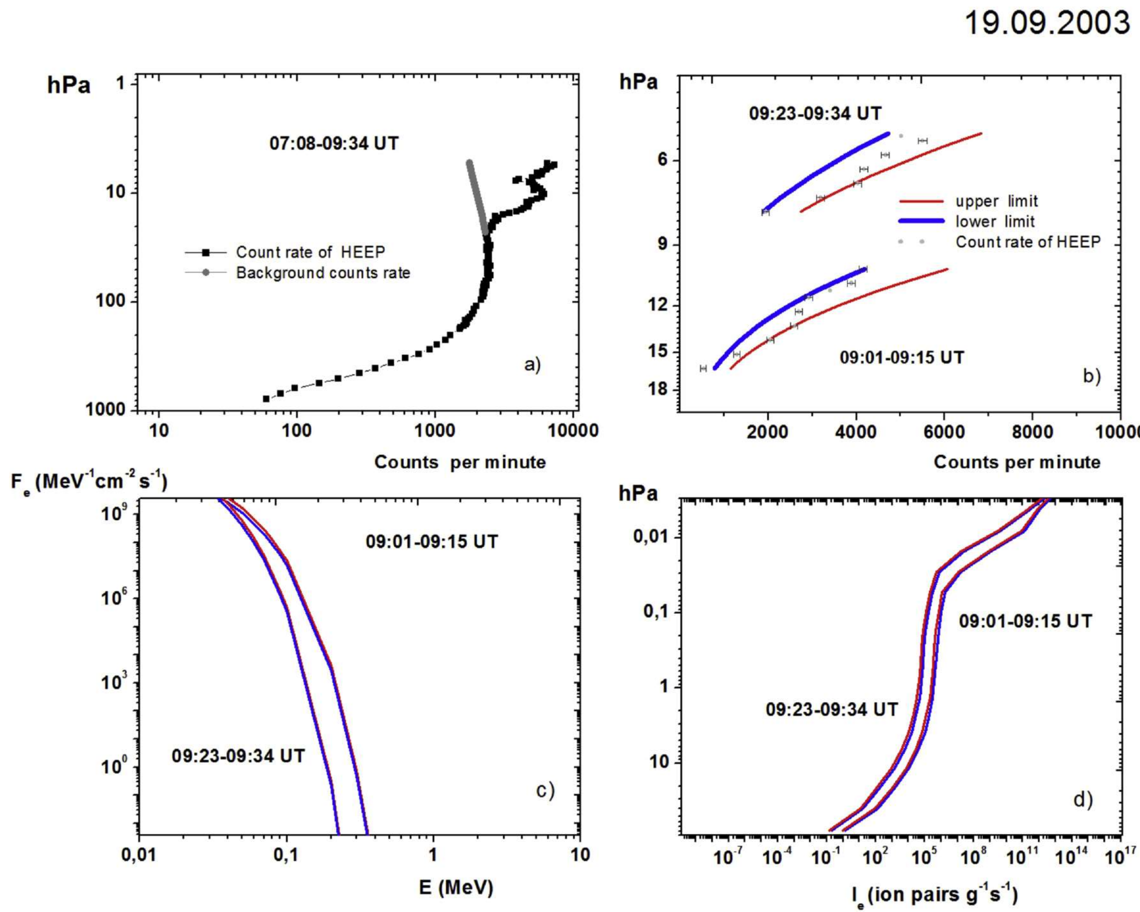
19.09.2003
hPa
07:08-09:34 UT
Count rate of HEEP
Background counts rate
a)
Counts per minute
09:23-09:34 UT
upper limit
lower limit
Count rate of HEEP
09:01-09:15 UT
b)
Counts per minute
F_e ($MeV^{-1}cm^{-2}s^{-1}$)
09:01-09:15 UT
09:23-09:34 UT
c)
E (MeV)
hPa
09:01-09:15 UT
09:23-09:34 UT
d)
I_e (ion pairs $g^{-1}s^{-1}$)

Figure 3

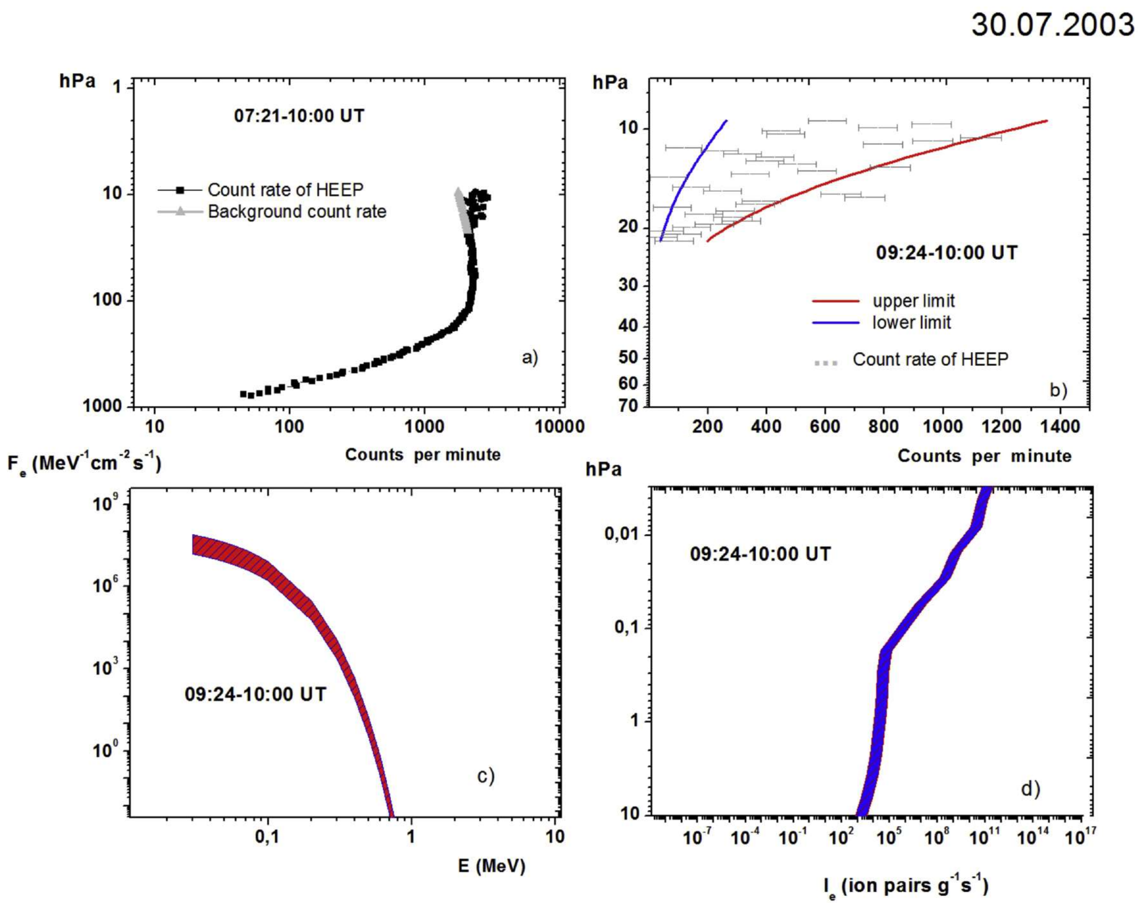

30.07.2003
hPa
07:21-10:00 UT
Count rate of HEEP
Background count rate
a)
Counts per minute
09:24-10:00 UT
upper limit
lower limit
Count rate of HEEP
b)
Counts per minute
F_e ($MeV^{-1}cm^{-2}s^{-1}$)
09:24-10:00 UT
c)
E (MeV)
hPa
09:24-10:00 UT
d)
I_e (ion pairs $g^{-1}s^{-1}$)

Figure 4

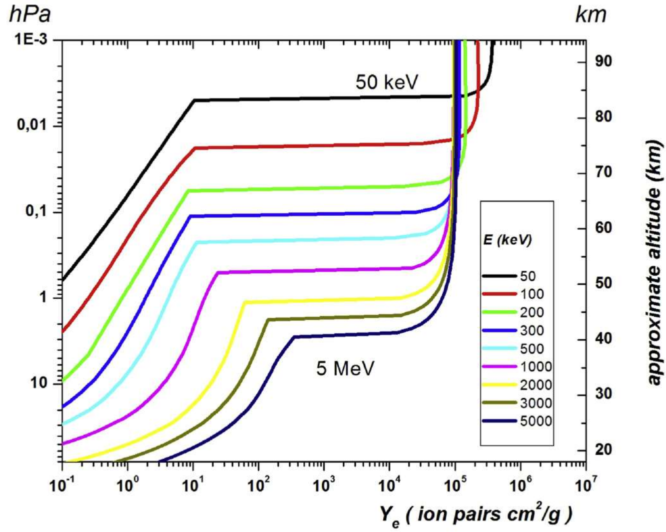

hPa
km
1E-3
0,01
0,1
1
10
90
80
70
60
50
40
30
20
50 keV
5 MeV
E (keV)
50
100
200
300
500
1000
2000
3000
5000
approximate altitude (km)
10^-1
10^0
10^1
10^2
10^3
10^4
10^5
10^6
10^7
Y_e (ion pairs cm^2/g)

Figure 5

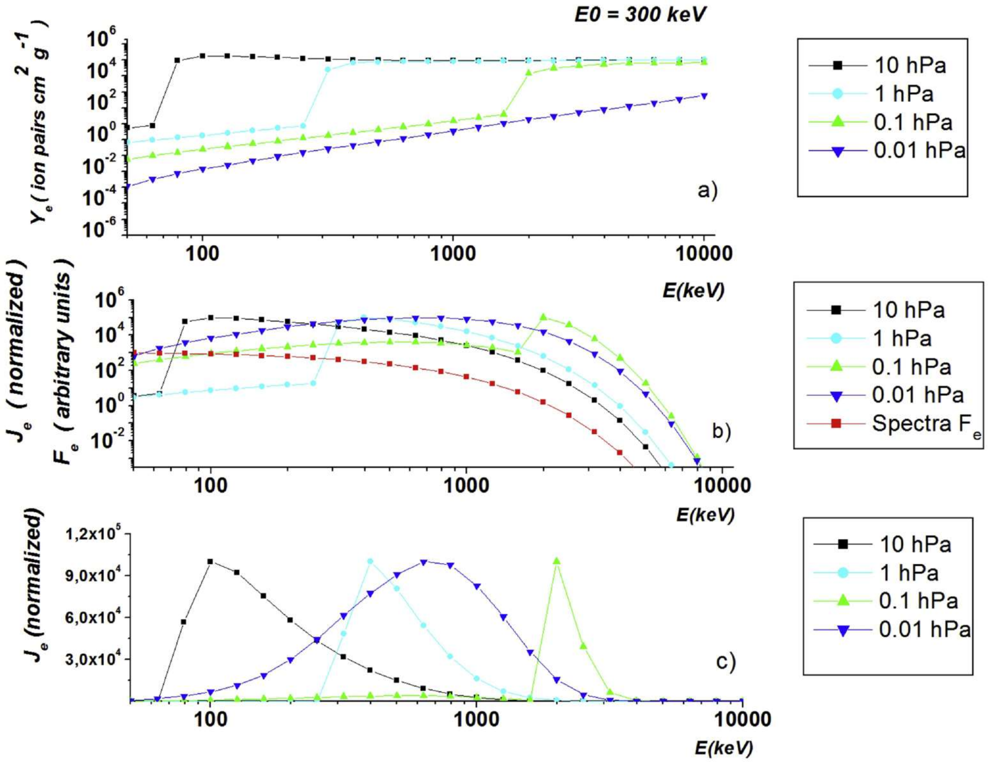
E0 = 300 keV
Y_e (ion pairs cm^2 g^{-1})
10 hPa
1 hPa
0.1 hPa
0.01 hPa
a)
E(keV)
J_e (normalized)
F_e (arbitrary units)
10 hPa
1 hPa
0.1 hPa
0.01 hPa
Spectra F_e
b)
E(keV)
J_e (normalized)
10 hPa
1 hPa
0.1 hPa
0.01 hPa
c)
E(keV)

Figure 6

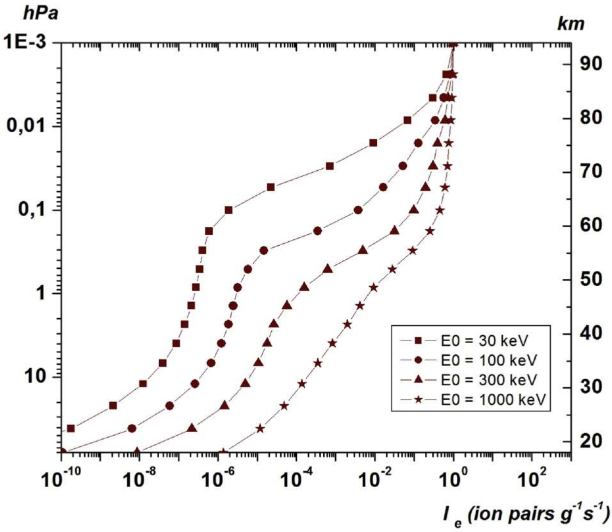
hPa
km
1E-3
0,01
0,1
1
10
90
80
70
60
50
40
30
20
approximate altitude (km)
E0 = 30 keV
E0 = 100 keV
E0 = 300 keV
E0 = 1000 keV
10^{-10}
10^{-8}
10^{-6}
10^{-4}
10^{-2}
10^{0}
10^{2}
I_e (ion pairs $g^{-1}s^{-1}$)

Figure 7

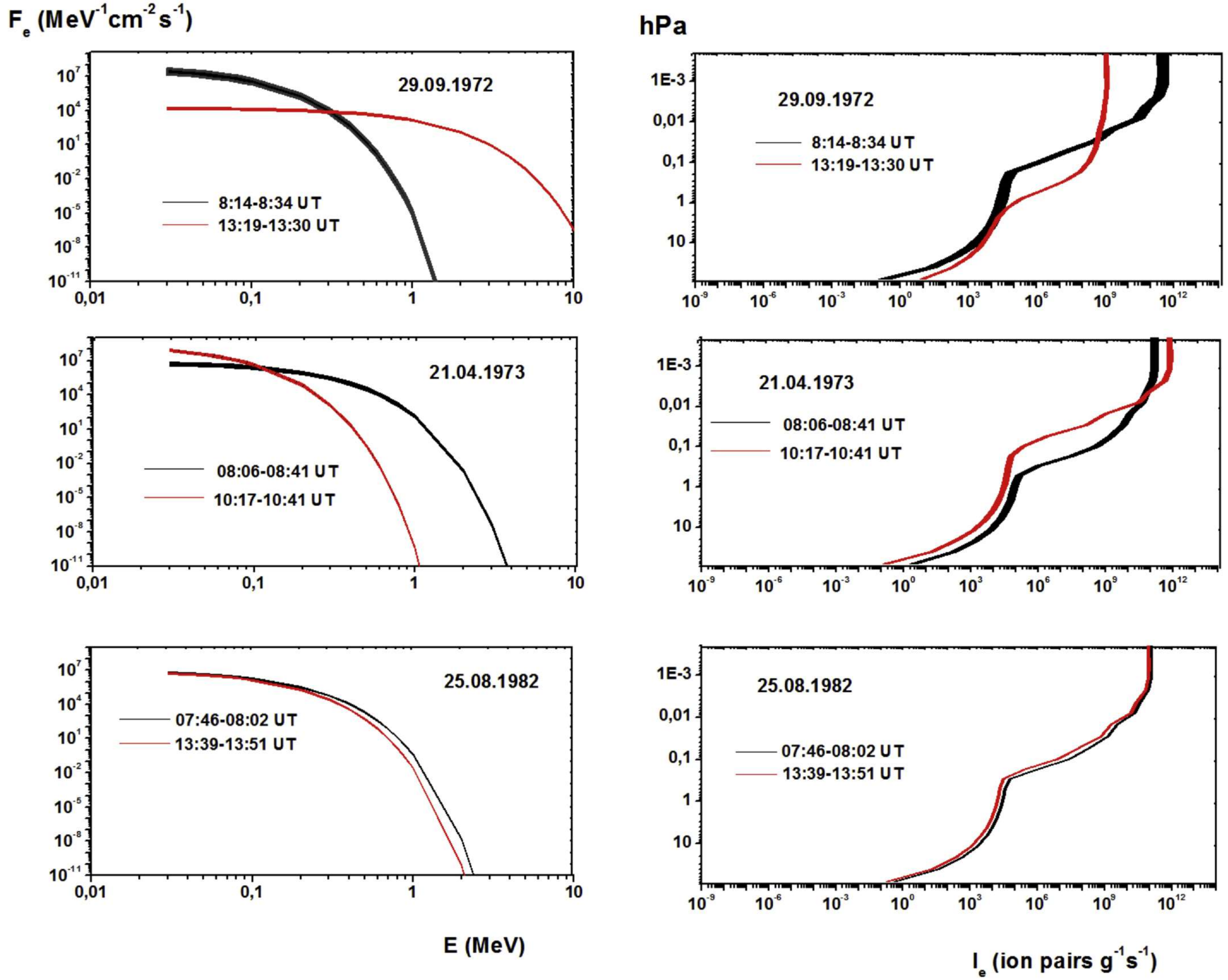

F_e (MeV^-1cm^-2s^-1)
29.09.1972
8:14-8:34 UT
13:19-13:30 UT
21.04.1973
08:06-08:41 UT
10:17-10:41 UT
25.08.1982
07:46-08:02 UT
13:39-13:51 UT
E (MeV)
hPa
I_e (ion pairs g^-1s^-1)

Figure 8